JOURNAL OF SOLID STATE CHEMISTRY 108, 158–163 (1994)

Structural Characteristics of Uniform γ-Fe_2O_3 Particles with Different Axial (Length/Width) Ratios

M. P. Morales, C. Pecharroman, T. Gonzalez Carreño, and C. J. Serna[1]

Instituto de Ciencia de Materiales de Madrid, C.S.I.C. Serrano 115 dpdo, 28006 Madrid, Spain

Received February 8, 1993; in revised form May 11, 1993; accepted May 17, 1993

Uniform particles of γ-Fe_2O_3 with axial (length/width) ratios from 1 (spheres) to 6.5 (ellipsoids) have been prepared by reduction–oxidation of α-Fe_2O_3. The particles are shown to be single crystals with their long axis collinear to the [111] crystallographic direction for the case of ellipsoidal particles. An increase in cation ordering was observed for γ-Fe_2O_3 as the axial ratio decreases, and the particles are completely ordered for spheres. It was observed that the extension of cation ordering in γ-Fe_2O_3 particles arises from the amount of defects present in the α-Fe_2O_3 precursor. These results could explain the differences in structural characteristics reported for γ-Fe_2O_3 by other authors depending on the experimental conditions.

INTRODUCTION

Due to its great technological importance for information recording systems and memory devices, γ-Fe_2O_3 has been widely studied (1, 2).

X-Ray diffraction data have established that γ-Fe_2O_3 possesses the same inverse spinel structure as magnetite (Fe_3O_4) but with some cation vacancies in octahedral positions. As a result, its formula can be written:

$$Fe^{3+}[Fe^{3+}_{5/3}[\quad]_{1/3}]\,O_4 \equiv Fe^{3+}_8[(Fe^{3+}_{4/3}[\quad]_{8/3})\,Fe^{3+}_{12}]\,O_{32}.$$

The ordering of these vacancies within the octahedral positions can give rise to several crystal symmetries for γ-Fe_2O_3 as indicated by differences in X-ray diffraction patterns. It has been suggested that the vacancies can be distributed: (1) at random (space group $Fd\bar{3}m$); (2) as the lithium cation in $LiFe_5O_8 \equiv Fe_8[Li_4\,Fe_{12}]\,O_{32}$ (space group $P4_132$); and (3) with an ordered distribution with tetragonal symmetry (space group $P4_32_12$) (1–5).

The origin of a particular cation distribution has been related to the preparation conditions. Thus, particles of γ-Fe_2O_3 formed by decomposition of γ-FeOOH have been reported to produce disordered structures (3), while particles formed by reduction–oxidation of α-Fe_2O_3 usually show some cation ordering (4, 5).

We have recently prepared uniform α-Fe_2O_3 particles of axial (length/width) ratios varying from 1 (spheres) to 6.5 (ellipsoids) in order to study their formation mechanism and crystallochemical characteristics (6). It was found that all the particles are monocrystalline, but with some defects, mainly as hydroxyl groups, which amount increases with the particle axial ratio as a consequence of their different growth mechanism (6).

We show here that the cation distribution in γ-Fe_2O_3 obtained from uniform α-Fe_3O_4 particles, may strongly vary with the particle axial ratio, i.e., with the amount of defects present in α-Fe_2O_3. Particular attention has been paid to the crystallochemical characteristics of the γ-Fe_2O_3 particles, i.e., single-crystal character and orientation of the crystallographic axes, due to their effects on the magnetic properties. A source of magnetic anisotropy in γ-Fe_2O_3 arises from the interaction of electron spins with the crystal structure of the oxide (1, 2).

EXPERIMENTAL

Preparation of γ-Fe_2O_3 Samples

Uniform γ-Fe_2O_3 particles with axial ratios from 1 to 6 were prepared from α-Fe_2O_3 samples of corresponding axial ratios reported in the Ref. (6). The conversion of α-Fe_2O_3 to γ-Fe_2O_3 was carried out through magnetite (Fe_3O_4) as the intermediate phase. For this purpose, α-Fe_2O_3 samples were maintained at 360°C between 3 and 4 hrs under hydrogen pressure (≈1 atm) to obtain pure Fe_3O_4 spinels. The reduction temperature was found to be critical as at slightly higher (370°C) or lower (350°C) values metallic iron or α-Fe_2O_3 phases were observed, respectively, in X-ray diffractograms. The Fe_3O_4 samples were later transformed to γ-Fe_2O_3 in an open furnace at 240°C for about 1 hr: Mössbauer spectra, ^{57}Co(Rh) as a source, were recorded to corroborate the absence of Fe^{2+}

[1] To whom correspondence should be addressed.

0022-4596/94 $6.00

TABLE 1
Characteristics of γ-Fe_2O_3 Uniform Particles

Sample	Axial ratio (length/width)	Crystallite size (Å) TEM	Crystalline size (Å) XRD (311)	S (m^2/g)
G-1	1.0 ± 0.1	1200 ± 100	2100 ± 300	5.8
G-2	1.8 ± 0.1	1650 ± 200 900 ± 100	1550 ± 200	8.2
G-3	3.0 ± 0.2	2950 ± 200 980 ± 100	1670 ± 200	9.0
G-6	6.3 ± 0.4	5300 ± 250 840 ± 100	1400 ± 100	9.5
G-SP	—	≤200 (aggregated)	200 ± 50	—

in the final γ-Fe_2O_3 samples. The uniform γ-Fe_2O_3 particles were designated according to their axial ratio (Table 1).

For comparison, a spherical γ-Fe_2O_3 sample composed of primary subunits in different agglomeration arrangements was also studied. The sample was produced by spray pyrolysis at 550°C from a 0.07 molar iron(III) nitrate solution (7). This sample was designated by G-SP (Table 1).

Structural Studies

The morphological characteristics of the particles were determined with a Philips 300 electron microscope. Particle size distributions were evaluated from the transmission electron micrographs by counting about 100 particles.

Lattice imaging coupled with selected area electron diffraction were carried out on individual particles with a 200-keV JEOL-2000 FXII electron microscope to determine monocrystalline character and orientation of the crystallographic axes.

Careful X-ray powder diffraction analyses were performed, between 10–30 2Θ on a Philips 1710 diffractometer using Fe$K\alpha$ radiation and a graphite monochromator, to determine superlattice reflections. Crystalline size determinations were carried out from X-ray diffractograms with Cu$K\alpha$ radiation following standard procedures (8).

Infrared spectra of the samples diluted in KBr were recorded between 850–250 cm^{-1} in a NICOLET 20SXC FTIR. For the far infrared region (600–100 cm^{-1}) the samples were dispersed in polyethylene and the spectra recorded with a NICOLET 20-F instrument.

Nitrogen adsorption isotherms were measured by an automatic volumetric apparatus at liquid nitrogen temperature. The BET method was applied to the surface area determination.

RESULTS AND DISCUSSIONS

The morphological characteristics of the samples are shown in Fig. 1 and Table 1. All studied samples were rather uniform in particle size and shape (monodispersed), with an average value in their particle thickness of about 900 Å (Table 1). Contrary expectation from unit-cell dimensions, a decrease in particle size was observed during the transformation of α-Fe_2O_3 to γ-Fe_2O_3 which must be attributed to some particle shrinkage during the reduction process.

A fairly good agreement was obtained between the particle sizes determined by X-ray diffraction with those observed by TEM (Table 1), suggesting that the particles preserve their monocrystalline character during the α-Fe_2O_3 to γ-Fe_2O_3 transformation. The high value in the particle size determined by X-ray diffraction for the case of spherical particles (sample G-1) is probably due to some particle sintering which was observed for this sample by TEM. In addition, the specific surface area of the samples, determined by nitrogen adsorption isotherms through the BET method, is within the order of magnitude of the surface area calculated from the sizes of the particles (≈10 m^2/g), under the assumption that the porosity is negligible. From a magnetic point of view, this is an interesting characteristic of the present particles because surface porosity and other types of defects are considered as sources of magnetic instability (9). In fact, when γ-FeOOH is converted to γ-Fe_2O_3 by heating at low temperature (<200°C), slit-shaped pores are formed along well-defined crystallographic planes (10, 11), with detriment to the magnetic properties.

A section of the X-ray powder diffraction patterns, including the region where most of the superlattice reflections appear, is illustrated in Fig. 2. It can be seen that the spherical γ-Fe_2O_3 particles (sample G-1) give reflections at 7.88, 6.92, 5.33, 4.28, and 3.20 Å which must be indexed on the basis of a tetragonal lattice with a = 8.33 Å and c/a = 3 (Table 2). These reflections can be interpreted according to the space group $P4_32_12$ as previously found by profile refinement of powder neutron diffraction data on an ordered γ-Fe_2O_3 sample (4). This tetragonal space group was based on the absence of the 002 reflections with $l \neq 4n$ which points to a fourfold screw axis with translation $c/4$.

With increase in particle axial ratio these superlattice reflections became less intense and broad, until they completely vanish for the sample G-6 (Fig. 2 and Table 2). A similar behavior is also observed for the reflections at about 5.88, 3.72, and 3.40 Å which correspond to the d_{110}, d_{210}, and d_{211}, respectively, of a primitive cubic lattice (space group, $P4_132$). Finally the sample prepared by spray pyrolysis (G-SP) presents only the (111) reflection at about 4.80 Å, characteristic of a disordered spinel structure (space group, $Fd\bar{3}m$).

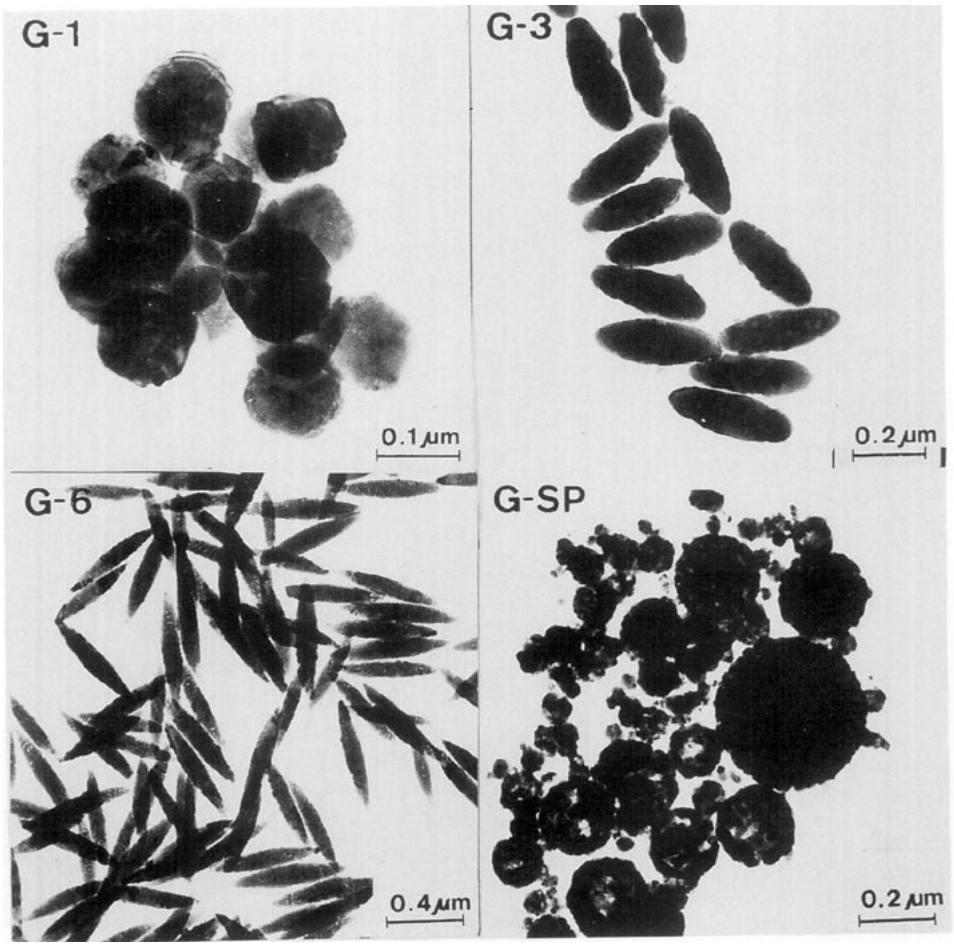

FIG. 1. Bright field TEM images of γ-Fe_2O_3: see Table 1.

Thus, a progressive cation disorder is found in γ-Fe_2O_3 with the increase in the axial ratio of the particles. A similar behavior has been also reported for Al-maghemites (γ-(Fe, Al)$_2O_3$) with variation in the amount of iron by aluminum substitution (5). However, in that case the lattice parameters were observed to decrease (from a = 8.34 Å to a = 8.31 Å and c = 25.2 Å to 24.9 Å) with the amount of iron substitution whereas here they remain rather constant (Table 2).

The infrared powder spectra of the γ-Fe_2O_3 samples also illustrate this order–disorder evolution with particle axial ratio (Fig. 3). An increases in the number of absorption bands is observed from the sample G-SP to G-1, in agreement to the decrease in symmetry of the particles, from $Fd3m$ (O_h^7) to $P4_32_12$ (D_4^8) (Table 3).

In general, the number of bands predicted for the different symmetries (ordering patterns) are greater than those experimentally observed, probably due to overlaping of some of the modes. An exception is present for sample G-SP, which suggests that the cation occupancies are not completely at random. It should be noticed that the frequency of any absorption band remains practically unaltered from sample G-SP to G-1. These results are rather analogous to those reported for γ-(Fe, Al)$_2O_3$ with increasing amount of aluminum (5, 12). However, for α-Fe_2O_3 significant differences have been observed in their infrared powder spectra with the amount of aluminum substitution (13) and also with the particle morphology (14). For the latter case, differences in frequency of some absorption bands greater than 100 cm^{-1} have been observed.

A schematic representation of the different types of octahedral cation distributions in the γ-Fe_2O_3 lattice is shown in Fig. 4. It illustrates the continuous cation ordering which exists in the γ-Fe_2O_3 particles, extending from the nearest neighbor cations for a cubic disordered spinel, up to the extended distances of a tetragonal cell with $c = 3a$.

A further question remains concerning the crystalline nature of the γ-Fe_2O_3 particles; i.e., whether every particle in each sample of γ-Fe_2O_3 is a single crystal or composed by a series of microcrystals chained together to

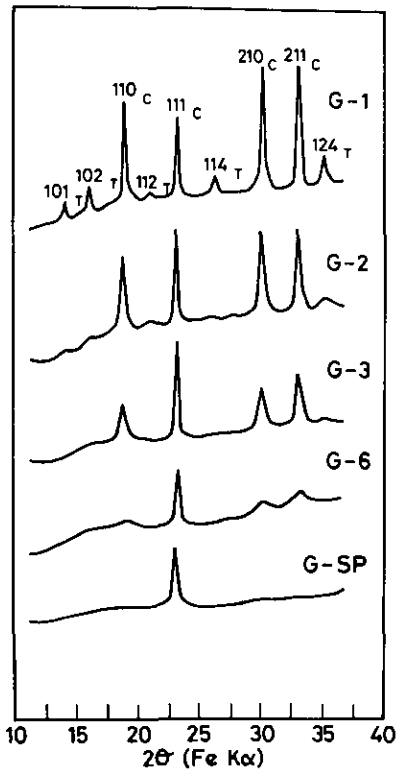

FIG. 2. X-ray diffraction patterns of γ-Fe_2O_3: see Table 1.

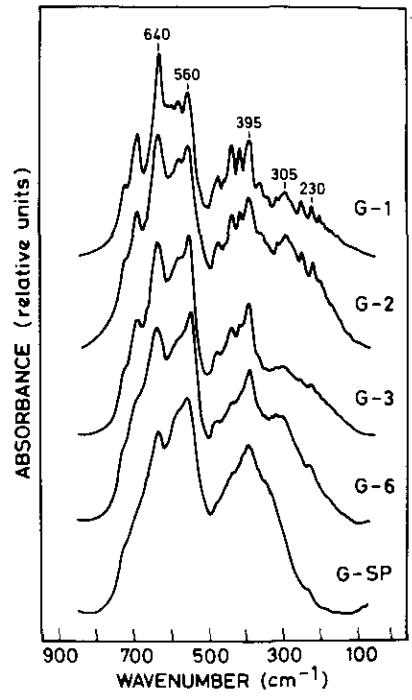

FIG. 3. Infrared powder spectra of γ-Fe_2O_3: see Table 1.

form a particle. For this purpose, lattice images and electron diffraction patterns on single particles with different axial ratios were carried out (Figs. 5–7). First of all, it should be noticed that all the samples studied gave diffraction patterns characteristic of monocrystalline particles; i.e., each particle behaves as a single crystal (Figs. 5–7). For the spherical particles, sample G-1, electron diffraction patterns show reflections which can be only indexed by a tetragonal cell. Thus, the reflections with spacing at 3.95, 2.66, and 1.97 Å correspond to the 202, 224, and 404 of a tetragonal cell, with a = 8.33 Å and $c = 3a$ (Fig. 5).

However, the observed reflections for sample G-3 at 5.90 and 4.82 Å would correspond with 110 and 111 of a primitive cubic lattice (Fig. 6). Analogously, characteristic reflections of a face-centered cubic lattice at 1.70 and 2.95 Å which corresponds to 224 and 220, are observed for sample G-6 (Fig. 7). The continuous increase in cation ordering suggested above as the particle axial ratio decreases, is mainfested in sample G-6 by the weak intensity reflections observed at 5.90 and 3.41 Å which must corre-

TABLE 2
X-Ray Diffraction Spacings of Different γ-Fe_2O_3 Samples (d = Å)

	Calculated[a]	G-1	G-2	G-3	G-6	G-SP
101_T	7.90	7.88	7.88			
102_T	6.93	6.92	6.93	6.93		
110_C	5.90	5.88	5.90	5.90	5.90	
112_T	5.33	5.33				
111_C	4.81	4.80	4.81	4.82	4.80	4.81
114_T	4.28	4.28				
210_C	3.72	3.72	3.72	3.72	3.72	
211_C	3.41	3.40	3.40	3.41	3.40	
124_T	3.20	3.20	3.20	3.20		

[a] Based on a tetragonal cell (a = 8.33 Å and $c = 3a$).

TABLE 3
Comparison between Observed and Calculated Vibrational Modes in γ-Fe_2O_3

Space group	$Fd\bar{3}m$ (O_h^7)	$P4_132$ (O^7)	$P4_32_12$ (D_4^8)
Atoms/primitive cell	14	56	160
Infrared active modes	4 F_{1u}	21 F_1	60 A_2 119 E
Contribution by oxygen movements	2 F_{1u}	9 F_1	36 A_2 72 E
Number of infrared observed modes	6 (G-SP)	16 (G-3)	24 (G-1)
Cation ordering	random	partially ordered	ordered

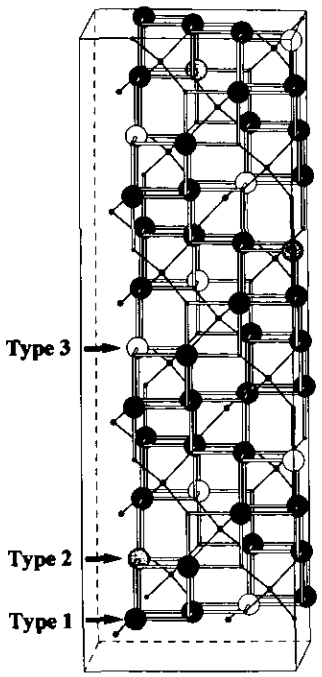

FIG. 4. Schematic representation of cation-vacancy ordering for the octahedral positions in γ-Fe_2O_3. Disordered γ-Fe_2O_3: all the positions are equivalent with a statistical occupation of 5/6 (space group, $Fd\bar{3}m$). Partially ordered γ-Fe_2O_3: Positions type 2 and 3 are equivalent with a statistical occupation of $\frac{1}{3}$. Position type 1 is completely occupied (space group, $P4_132$). Ordered γ-Fe_2O_3: all the vacancies are in position type 3. Positions type 1 and 2 are completely occupied (space group, $P4_32_12$).

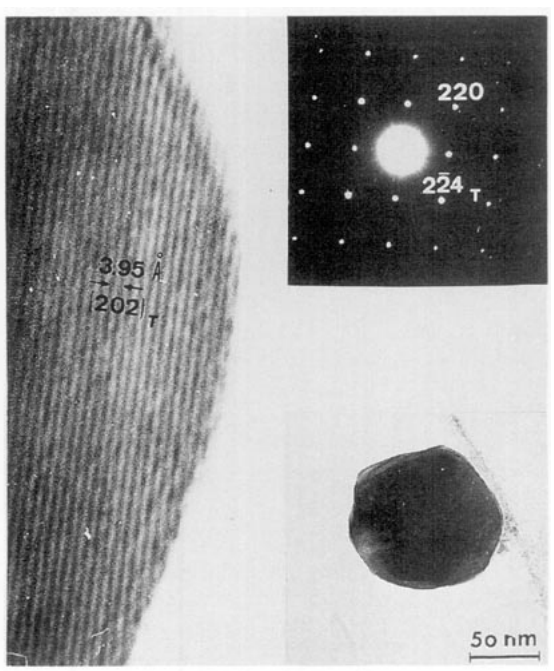

FIG. 5. Lattice image and diffraction pattern for sample G-1 taken from incident [111].

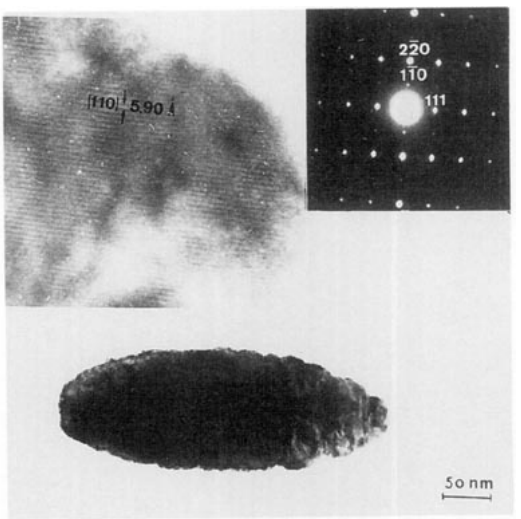

FIG. 6. Lattice image and diffraction pattern for sample G-3 taken from incident [112].

spond to 110 and 211, respectively, of a primitive cubic lattice (Fig. 7).

For the case of ellipsoidal particles, the long axis was found to be coincident to the [111] direction (Figs. 6 and 7). This is consistent with a topotactic transformation from α-Fe_2O_3 crystals which have their long axis parallel to [001] (6). However, other orientations have been reported for the long axis of anisometric particles of γ-Fe_2O_3, because the precursor α-Fe_2O_3 crystals had different crystallographic orientation (1, 15).

The continuous increase in cation ordering observed in γ-Fe_2O_3 with decrease of the particle axial ratio must be attributed to the presence of defects, some as hydroxyl

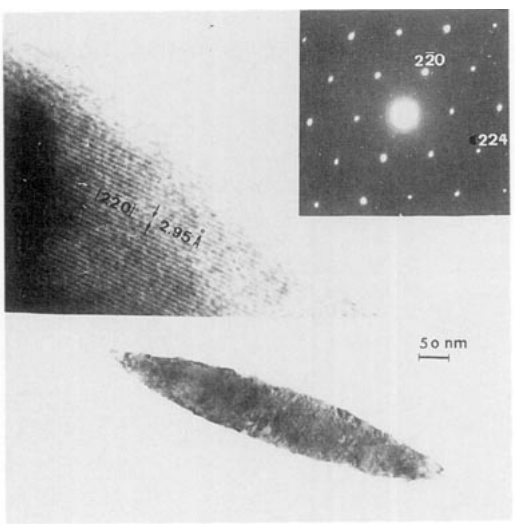

FIG. 7. Lattice image and diffraction pattern for sample G-6 taken from incident [111].

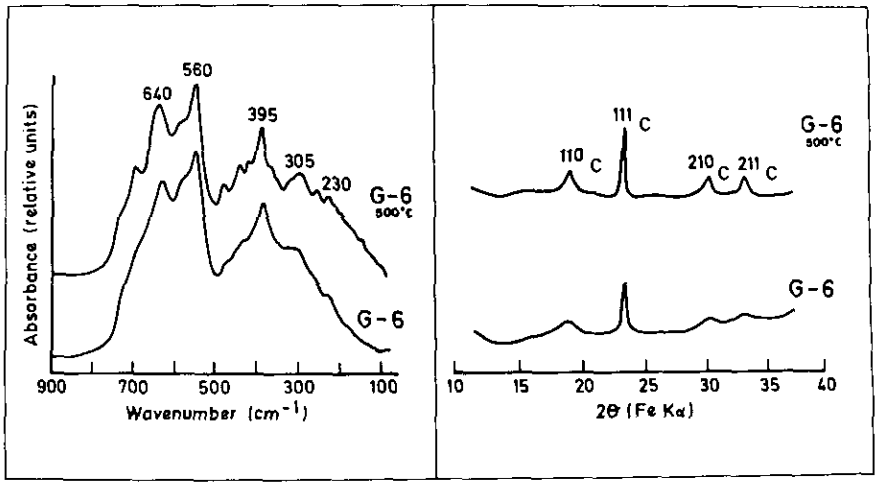

FIG. 8. X-ray diffraction patterns (right) and infrared powder spectra (left) of: γ-Fe_2O_3 prepared from unheated α-Fe_2O_3 (sample G-6) and γ-Fe_2O_3 prepared from the same α-Fe_2O_3 sample but initially heated at 500°C for 3 days.

groups or water molecules, previously found in α-Fe_2O_3, which also increase with the particle axial ratio (6). In order to test this hypothesis γ-Fe_2O_3 particles were prepared in the manner of sample G-6 but with a previous heating of the α-Fe_2O_3 precursor at 500°C for 3 days to eliminate some of the defects. At this temperature the α-Fe_2O_3 precursor particles lose about 4% in weight without altering their morphology (6). A comparison between the sample G-6 and the one obtained by previous heating of α-Fe_2O_3 shows that an improvement in cation ordering takes place (Fig. 8). This result clearly illustrates that the defects present in α-Fe_2O_3 are responsibles for the order–disorder characteristics of the final γ-Fe_2O_3 obtained and may be the final reason for the different types of ordering found in γ-Fe_2O_3 particles depending on experimental conditions.

ACKNOWLEDGMENTS

M. P. Morales and C. Pecharroman gratefully acknowledge their fellowships from the Ministerio de Universidades e Investigacion. This research was supported by the CICYT under Project MAT-93-0789.

REFERENCES

1. G. Bate, in "Ferromagnetic Materials" (E. P. Wohlfarth, Ed.) pp. 381–507. North-Holland, Amsterdam 1980.
2. M. P. Sharrock, *IEEE Trans. Magn.* **25,** 4374 (1989).
3. R. Giovanoli and R. Brutsch, *Thermochim. Acta* **13,** 15 (1975).
4. C. Greaves, *J. Solid State Chem.* **49,** 325 (1983).
5. E. Wolska and U. Schwertmann, *Solid State Ionics* **32–33,** 214 (1989).
6. M. P. Morales, T. Gonzalez-Carreño, and C. J. Serna, *J. Mater. Res.* **7,** 2538 (1992).
7. F. T. Gonzalez-Carreño, M. P. Morales, M. Gracia, and C. J. Serka, *Mater. Lett.* (in press).
8. L. U. Azaroff, in "Elements of X-ray Crystallography." McGraw–Hill, New York (1968).
9. S. J. Andress, A. Benedetti, A. R. Corradi, and G. Fagherazzi, *IEEE Trans. Magn.* **22,** 1341 (1986).
10. H. Naomo, R. Fugiwara, H. Sugioka, K. Sumiya, and H. Yanazawa. *J. Colloid Interface Sci.* **87,** 317 (1989).
11. J. L. Rendon, J. Cornejo, P. de Arambarri, and C. J. Serna, *J. Colloid Interface Sci.* **92,** 508 (1983).
12. B. Gillot, *Mater. Chem. Phys.* **10,** 375 (1984).
13. Barron V., J. L. Rendon, J. Torrent, and C. J. Serna, *Clays Clay Miner.* **32,** 475 (1984).
14. C. J. Serna, M. Ocaña, and J. E. Iglesias, *J. Phys. C.* **20,** 473 (1987).
15. G. W. van Oosterhout, *Acta Crystallogr.* **13,** 932 (1960).